The open-framework structure of KSbGe3O9 flux-grown crystals investigated by X-ray diffraction, vibrational spectroscopy, and DFT calculations

Monique Tillard, P Hermet, A Haidoux, D Granier, Pascale Armand

The open-framework structure of $KSbGe_3O_9$ flux-grown crystals investigated by X-ray diffraction, vibrational spectroscopy, and DFT calculations.

M. Tillard, P. Hermet, A. Haidoux, D. Granier, P. Armand*

ICGM, Université de Montpellier, CNRS, Montpellier, France

Corresponding author

*E-mail : pascale.armand@umontpellier.fr; Tel : +33 (0)4 67 14 33 19

ORCID : 0000-0001-8921-5427.

Abstract

We report on the preparation and the X-ray crystal structure of colorless $KSbGe_3O_9$, its vibrational properties (Raman and infrared studies), and density functional theory (DFT) calculations. $KSbGe_3O_9$, grown by the high-temperature flux method from $K_2Mo_4O_{13}$ flux, is thermally stable at least up to 1200°C and is isostructural to the benitoite $BaTiSi_3O_9$ (space group $P\bar{6}c2$ (n°. 188)). The hexagonal unit cell contains two formula units and the structure was refined to $R1$ = 0.0324 from single-crystal X-ray diffraction data. $KSbGe_3O_9$ is characterized with only one crystallographically independent Ge atom involved in three-member units $[Ge_3O_9]^{6-}$ of regular germanate tetrahedra. The K^+ ions are located in channels and, like Sb^V, are octahedrally surrounded by oxygen atoms. The $KSbGe_3O_9$ local structure and the planarity of Ge_3O_3 rings are also studied by a room-temperature vibrational investigation using non-polarized infrared and Raman spectroscopy. Both the infrared and Raman phonon modes have been assigned from the agreement observed between our experimental data and the corresponding DFT ones. In particular, two E'(TO) modes (both IR and Raman active) characterize the planarity of the Ge_3O_3 ring in the *ab* plane.

KEYWORDS:

A.oxide materials, C.crystal structure, C.phonons, D. computer simulation, D. optical spectroscopy, D.X-ray diffraction

1. INTRODUCTION

Non-centrosymmetric germanate crystals with large nonlinear optical (NLO) properties are potential materials in the area of photonics and optical devices as they present electro-optical effects and second-order harmonic generation capabilities which able them to switch an optical signal and to generate light with a frequency twice as the fundamental laser light [1-3]. Non-centrosymmetric germanate may also present interesting piezoelectric properties which are appropriate for volume- or surface-acoustic wave devices [4, 5]. In this context, the searching and the development of transparent and colorless germanate single-crystals with a non-centrosymmetric structure and enhanced properties are important. For industrial applications in a harsh environment (with T > 600°C), lead-free materials that can operate under extreme stress without degradation should have a stoichiometric chemical composition and structural stability in a large thermal domain as encountered for the non-polar uniaxial α-GeO_2 single crystal [6, 7].

Based on the relationship between the tunnel structure and the physical properties of acentric germanate frameworks [8, 9], we have been interested in the $AMGe_3O_9$ family with a monovalent or bivalent (A = K, Rb, Ba, Ca, Tl) and a pentavalent or tetravalent (M = Sn, Nd, Ti, Ta) chemical element. These oxides which display the benitoite-type structure are characterized by a mixed framework built with MO_6 octahedra and GeO_4 tetrahedra, the latter forming a 3-member ring $[Ge_3O_9]^{6-}$ with C_{3h} symmetry [10-15]. The GeO_4 units are known as microscopic NLO-active motifs and, when associated with a strongly electropositive alkaline element, the NLO efficiency of such oxide could be improved [16]. Furthermore, these double germanate with an open-framework structure and well-defined channels may be suitable for ion-exchange and gas adsorption applications.

This paper reports on the spontaneous crystallization of the compound $KSbGe_3O_9$ using the high-temperature flux method and on its single crystal structure determination associated with a

vibrational characterization. The experimental study is completed by a group theory analysis and density functional theory (DFT) calculations to investigate the $KSbGe_3O_9$ infrared (IR) and Raman spectra.

2. TECHNICAL SECTION

Crystals were obtained using the flux method described elsewhere [17]. For the present study, $K_2Mo_4O_{13}$ was chosen as flux and synthesized via a solid-state reaction at 500°C for two weeks, from alkali carbonate K_2CO_3 and molybdenum oxide MoO_3 powders. The compound was characterized through classical methods and more precision on the conditions for EDX, spectroscopy, or X-ray diffraction experiments can be found in our previous paper [17].

Calculations on $KSbGe_3O_9$ have been performed within the density functional theory (DFT) framework as implemented in the ABINIT package [18]. The all-electron potentials are replaced by norm-conserving pseudopotentials generated according to the local density approximation [19]. K ($4s^1$), Sb ($5s^2$, $5p^3$), Ge ($4s^2$, $4p^2$) and O ($2s^2$, $2p^4$)-electrons are considered as valence states. The electronic wave functions are expanded in plane-waves up to a kinetic energy cutoff of 65 Ha and the integrals over the Brillouin zone were approximated by sums over an 8×8×6 mesh of special k-points according to the Monkhorst-Pack scheme [20]. The lattice parameters and the atomic positions were fully relaxed using a Broyden-Fletcher-Goldfarb-Shanno algorithm until the maximum stresses and residual forces were less than 2×10^{-4} GPa and 6×10^{-6} Ha/Bohr, respectively. Born effective charges, dielectric tensors, and dynamical matrix (yielding the phonon frequencies and eigenvectors) were obtained within a variational approach of the density functional perturbation theory, whereas the Raman susceptibilities were calculated from a nonlinear response formalism taking advantage of the $2n+1$ theorem [21].

3. RESULTS AND DISCUSSION

3.1 Flux-growth result

Visually transparent and colorless as-grown crystals of almost millimeter size were obtained via spontaneous nucleation from the high-temperature flux method. Their chemical analysis shows the presence of only Ge, K, and Sb in atomic ratios K/Sb of 1 and Ge/Sb of 3 which gives the nominal composition $KSbGe_3O_9$. DSC measurement from room temperature to 1200°C with a 10°/min heating rate did not point out any endo- or exo-thermal event. This means that the structure of $KSbGe_3O_9$ is thermally stable at least up to 1200°C and that its melting temperature is over 1200°C.

Figure 1 shows the X-ray diffraction pattern θ-2θ scan registered at room temperature for $KSbGe_3O_9$. The reflections can be indexed within the hexagonal $P\bar{6}c2$ space group (188) according to the JCPDS card number 00-038-1334 [22]. A small reflection attributed to the flux $K_2Mo_4O_{13}$ is present on the X-ray diffraction pattern (indicated by an arrow).

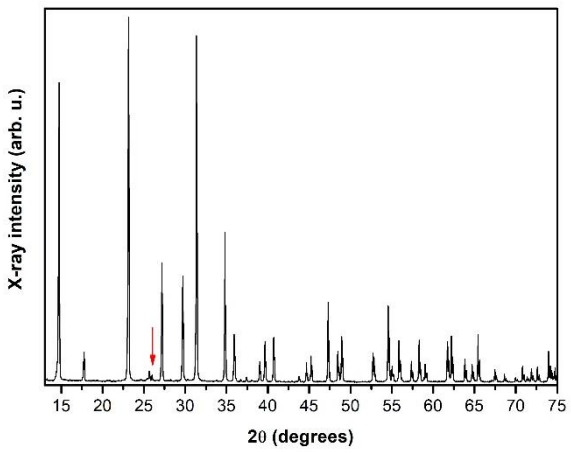

Figure 1: Powder X-ray diffraction pattern of $KSbGe_3O_9$ crushed sample.

3.2. X-ray crystal structure.

The as-grown transparent platelets are not single-crystals as they look bright in any orientation under polarized light. Attempts were made to carefully cut them into smaller single-crystals, but it rapidly became obvious that the resulting fragments still consisted of several crystalline components. This was clear from the X-ray diffraction images characterized, by at least, two reciprocal lattices. However, two specimens selected under a stereomicroscope equipped with a polarizing filter were used to record diffracted intensities. Because such twinning occurs by very weak offset in the *ab* plane (as can make the pages of a book), a multi-crystal treatment of the data (reflections were too close to be separated) or the use of a twinning law have been impossible.

The structure was solved and further refined by the full-matrix least-squares method using the SHELXTL software package [23, 24]. The positional and anisotropic displacement parameters have been refined for all atoms using all the measured reflections in refinements on F^2. The total filling of the atomic sites has been checked by a free refinement of the occupational factors which did not deviate from unity within the standard deviation limits.

The main crystal data and refinement parameters are given in Table 1 while the atomic positions and the equivalent displacement parameters are listed in Table 2. The full CIF files (CCDC numbers 1990049-50) can be obtained free of charge from the Cambridge Crystallographic Data Center [25].

Table 1. Crystal structure and refinement parameters for the two studied crystals of $KSbGe_3O_9$.

Space group	$P\bar{6}c2$ (188)	
Temperature (K)	298 (2)	
Diffractometer, radiation	Bruker D8 Venture, Kα Mo	
Wavelength (Å)	0.7107	
Lattice (Å)	*a* = 6.9436(1), *c* = 9.9934(2)	*a* = 6.9527(1), *c* = 10.0117(2)
Volume ($Å^3$)	419.13(2)	418.27(2)
Z	2	
Density (g/cm^3)	4.14	4.15
μ (mm^{-1})	14.4	
Absorption correction	multi-scan method (SADABS)	
Crystal (mm)	0.086×0.085×0.042	0.10×0.08×0.03
θ range (°)	3.39 - 62.22	3.38 - 72.37
Index ranges	-16≤h≤17, -17≤k≤17	-17≤h≤18, -18≤k≤18
	-24≤l≤24	-26≤l≤26
Collected reflections	40471	69478
Independent reflections	2313 [R_{int} = 0.0568]	2886 [R_{int} = 0.0522]
Goodness-of-fit on F^2	1.271	1.132
Final R indices [I > 2σ(I)]	R1 = 0.0324, wR2 = 0.0578	R1 = 0.0233, wR2 = 0.0550
R indices (all data)	R1 = 0.0377, wR2 = 0.0592	R1 = 0.0245, wR2 = 0.0552
Absolute structure parameter	0.043(16)	0.083(11)
Extinction coefficient	0.044(3)	0.040(3)
Δρ Fourier residuals ($e.Å^{-3}$)	3.49 / -1.72	2.29 / -1.96

Table 2. Atomic coordinates and equivalent displacement parameters ($Å^2×10^5$) for $KSbGe_3O_9$ (*italics* for crystal 2). U_{eq} is defined as ⅓ of the trace of the orthogonalized U_{ij} tensor.

	x	y	z	U_{eq}
Sb	0	0	0	613(3)
	0	*0*	*0*	*686(4)*
Ge	0.12135(3)	0.37281(3)	0.25	706(1)
	0.12133(4)	*0.37280(4)*	*0.25*	*784(4)*
K	0.66667	0.33333	0	3850(5)
	0.66667	*0.33333*	*0*	*3840(5)*
O1	0.0663(3)	0.5931(3)	0.25	1560(3)
	0.0668(3)	*0.5935(3)*	*0.25*	*1620(4)*
O2	0.2411(3)	0.0136(4)	0.1071(2)	2690(3)
	0.2409(4)	*0.0140(4)*	*0.1073(2)*	*2730(4)*

For both crystals, the recorded reflections have been indexed in a primitive hexagonal lattice ($a = b \approx 7$, $c \approx 10$ Å) and the statistical tests on intensities indicated a non-centrosymmetric space group. But, because the structure of $KSbGe_3O_9$ was previously reported, from X-ray powder diffraction studies, with the larger hexagonal cell $a = b = 13$ Å and $c = 10$ Å in the $P\bar{6}c2$ space group [22], we also tried to index our data in a 2×2×1 supercell, which gives rise to additional reflections ($h = 2n+1$) of extremely low intensity and high σ(I) values. No solution was found in this supercell and the refinement of a model built from twice the sub-cell structure did not converge either properly, giving arguments to reject a parameter doubling.

Furthermore, structure solutions have been found in the basic cell of parameters $a=b \approx 7$, $c \approx 10$ Å, and those obtained in the most probable space groups differ only by the *z*-coordinates of Ge and O atoms. Constrained by the symmetry in $P\bar{6}c2$ ($z = 0$ or 0.25) or free to vary in $P3c1$, they lead to Ge_3O_3 rings either flat or wavy. Refinement of the structural model in the lower symmetry $P3c1$ (which allows the greatest freedom degree) conducted for both crystal data sets shows that the deviation, with regard to the plane, remains lower than 0.007Å within the Ge_3O_3 planar rings. This behavior is also reflected in the atomic displacement parameters of the O1 atoms, "frozen" in the planar rings, which are lower than those of the O2 atoms, covalently bonded in “softer” Ge-O-Sb bridges, and those of K atoms present as cations involved in weaker ionic interactions. In these conditions, the structure is given in the highest hexagonal symmetry $P\bar{6}c2$ usually reported for the $AMGe_3O_9$ compounds [10-15]. The choice of this space group is also supported by careful analysis of the powder diffraction data, Figure 1, which indicates no lowering of the symmetry, thus eliminating merohedral twinning (true crystal symmetry $P31c$) which would result in the perfect overlap of the reciprocal lattices. An essential characteristic in the structure of $KSbGe_3O_9$ lies in the flatness of the Ge_3O_3 rings, a situation differing from $RbSbGe_3O_9$ which a structural study has just been published [17].

The compound $KSbGe_3O_9$ is isostructural with the benitoite $BaTiSi_3O_9$ which is known as a structural type [10, 11, 15]. It is characterized by SbO_6 octahedra and GeO_4 tetrahedra which arrangement provides $[Ge_3O_9]^{6-}$ units formed with Ge_3O_3 planar rings (see in Figure 2 the structure representations drawn using Diamond software [26]). The relevant interatomic distances and angles in this three-dimensional open-framework structure are given in Table 3. The non-distorted SbO_6 octahedra share its vertices with six GeO_4 tetrahedral units, the latter display regular tetrahedral geometry and share vertices with two GeO_4 tetrahedra and two SbO_6 octahedra. The SbO_6 octahedra are separated by Ge_3O_3 rings. The voids between the polyhedra, filled with K atoms, form channels along the *c*-axis.

The atomic arrangement in $KSbGe_3O_9$ can also be viewed as composed of two planes of Ge_3O_3 rings perpendicular to the *c* axis (at z = 0.25 and z = 0.75) followed, above and below, by an oxygen layer and then a layer containing both Sb and K atoms.

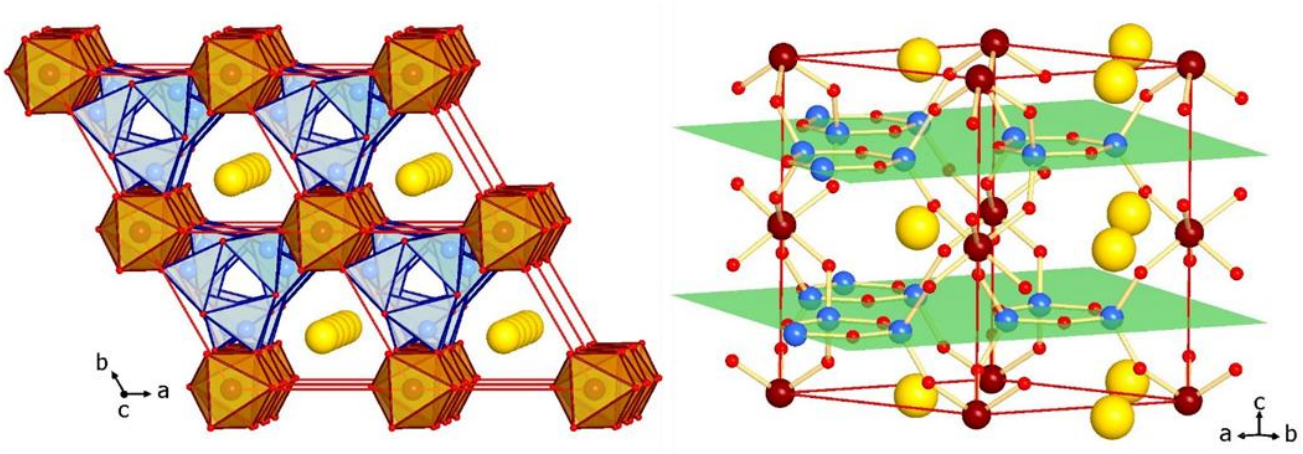

Figure 2. Structural representations of $KSbGe_3O_9$ emphasizing: *left*-the GeO_4 (blue) and SbO_6 (brown) regular polyhedral packing forming channels containing the K^+ ions (yellow). *right*-the Ge_3O_3 planar rings in the *ab* plane.

Table 3. Selected bond lengths (Å) and angles (°) for $KSbGe_3O_9$

Sb-O2	1.949(2) × 6	O1-Ge	1.741(2)
		O1-Ge	1.754(2)
K-O2	2.875(2) × 6	Ge-O2	1.731(2) ×2
		Ge-O1	1.741(2)
O2-Sb-O2	83.9(1) × 3	Ge-O1-Ge	129.6(1)
O2-Sb-O2	175.0(2) × 3	Ge-O2-Sb	134.61(1)
O2-Sb-O2	92.6(1) × 6	O2-Ge-O2	111.1(2)
O2-Sb-O2	91.1(2) ×3	O2-Ge-O1	114.3(1) × 2
		O2-Ge-O1	102.7(1) × 2
		O1-Ge-O1	110.4(1)

3.3. Vibrational properties

The zone-center optical phonons of $KSbGe_3O_9$ can be classified according to the irreducible representations of the D_{3h}-point group as $7A'_1 \oplus 9A'_2 \oplus 6A''_2 \oplus 5A''_1 \oplus 15E' \oplus 12E''$. The A'_2 and A''_1 modes are silent. The E'-representation is both infrared and Raman active while the E''-representation is only Raman active. The A''_2 (resp. A'_1) representation is infrared (resp. Raman) active.

The room-temperature infrared (450 - 1100 cm^{-1}) and Raman (100 – 1100 cm^{-1}) spectra of the non-centrosymmetric $KSbGe_3O_9$ material are presented in Figure 3. Five main infrared bands can be identified (Fig. 3a) at 498, 570, 798, 841, and 920 cm^{-1}. Similarly, thirteen Raman can be observed (Fig. 3b) at 113, 164, 207, 222, 268, 323, 439, 485, 527, 562, 838, 913 and 940 cm^{-1}. All these contributions are in agreement with the literature reports [27]. Our DFT based calculations support these experimental features (Fig. 3) and their assignment is listed in Table 4 along with additional experimental infrared/Raman bands with small or very small intensity. This agreement between the

experimental vibrational spectra and the theoretical ones support our structure refinement for the non-centrosymmetric $KSbGe_3O_9$ material and points out the high quality of the as-grown crystals.

The silent frequencies calculated at 0 K for the $KSbGe_3O_9$ crystal (D_{3h} point group, lattice parameters a = 6.9436(1) Å, c= 9.9934(2) Å) are listed in Table 5.

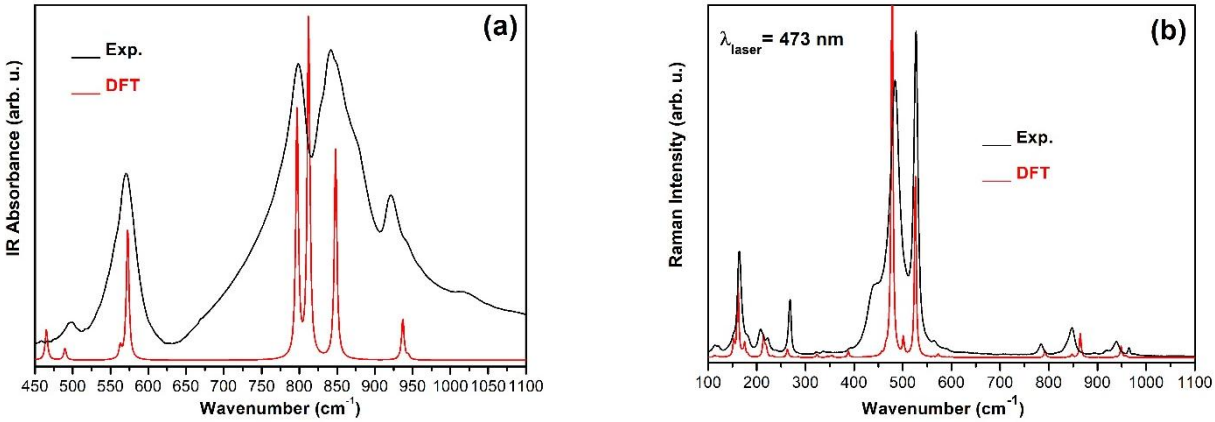

Figure 3: Room-temperature experimental and 0 K-calculated (a) infrared (KBr-pellet method) and (b) Raman spectra of the $KSbGe_3O_9$ crushed sample.

Table 4. Position of the experimental and calculated optical modes (infrared and Raman) with their Mulliken symmetry for $KSbGe_3O_9$ in the D_{3h} point group.

Calculated wavenumbers (cm^{-1})	Symmetry	Observed wavenumbers (cm^{-1})	
		Raman Expt.	Infrared Expt.
65	E" (TO)		
68	$A"_2$ (TO)		
75	$A"_2$ (LO)		
92	E" (TO)		
111	E' (TO, LO)	108	
114	E' (TO)	113	
115	E" (TO)	118	
121	E' (LO)		

133	A”$_2$ (TO)		
137	A”$_2$ (LO)		
153	E” (TO)	158	
161	A’$_1$ (TO)	164	
170	E’ (TO, LO)	168	
175	E” (TO)	174	
181	E” (TO)	183	
213	E’ (TO)	207	
220	E’ (LO)	222	
233	E’ (TO, LO)	233	
259	A”$_2$ (TO)		
263	A’$_1$ (TO)	268	
267	E’ (TO)	278	
274	E’ (LO)		
285	E” (TO)	300	
324	E’ (TO)	323	
326	A”$_2$ (TO, LO)		
333	A”$_2$ (LO)		
345	E” (TO)		
355	E’ (LO)		
388	A’$_1$ (TO)	392	
427	E’ (TO)	439	
432	E’ (LO)		
457	E” (TO)		
465	E’ (TO)	464	498
473	E’ (LO)		
478	A’$_1$ (TO)	485	
490	A”$_2$ (TO)		
495	A”$_2$ (LO)		
501	E” (TO)	495	
526	A’$_1$ (TO)	527	
563	E’ (TO, LO)	562	
572	E’ (TO)	566	570
602	E’ (LO)		
792	E” (TO)	787	
797	E’ (TO)	795	798

812	A”$_2$ (TO)		798
818	E’ (LO)		
848	E’ (TO)	838	841
863	A’$_1$ (TO)	849	
864	E” (TO)	849	
901	E’ (LO)		878
930	A”$_2$ (LO)		
937	E’ (TO)	913	920
944	E’ (TO, LO)	919	943
948	A’$_1$ (TO)	940	
959	E’(LO)		
			1018*

* Combination band

Table 5. A’$_2$ and A”$_1$ silent mode position for $KSbGe_3O_9$ in the D_{3h} point group.

Symmetry	Calculated wavenumbers (cm^{-1})
A’$_2$	74
A’$_2$	145
A”$_1$	156
A’$_2$	213
A”$_1$	240
A’$_2$	251
A”$_1$	350
A’$_2$	408
A’$_2$	473
A”$_1$	495
A’$_2$	527
A’$_2$	858
A’$_2$	915
A”$_1$	965

3.4. Vibrational frequency assignments.

The structural origin of the vibrational components was interpreted using the results of the density functional theory calculations. Only the most intense IR and Raman vibrational bands were investigated. The theoretical vibrations in the range 450 - 1000 cm^{-1} are mainly due to the oxygen motions and, for some of them, to the vibrations of the Ge atoms in a small content. Within the Ge_3O_9 cyclic unit, there are two types of oxygen atoms (see Table 2): the bridging O (O1) bonded to two Ge atoms (Ge-O1-Ge forming the Ge_3O_3 planar ring) and the non-bridging O (O2) bonded to one Ge atom (Ge-O-K/Sb).

The first intense Raman line is found at 478 cm^{-1} by DFT calculation against 485 cm^{-1} experimentally, Figure 3b and Table 5. This mode is assigned as A'_1 and it is only Raman active. This vibration is mainly caused by the symmetric stretching of O2-K "pairs", which leads to the bending of the O2-Sb-O2 angle. In this mode, the K atoms are fixed and the Ge atoms too, Figure 4.

The 563 cm^{-1} calculated frequency which is both IR and Raman active (E'(TO), Table 5) is due to Ge-O1-Ge intra-cycle bending motions in the Ge_3O_3 ring and to the O2-K-O2 wagging motion of the KO_6 octahedra, Figure 4. Both O and Ge atoms participate in this vibration mode while K and Sb atoms are fixed. This band characterizing the annular units appear in the IR/Raman spectra at a frequency of 500-570 cm^{-1} in three-membered rings germanates and is called the "ring band" [27, 28, 29].

Concerning the 797 cm^{-1} E'(TO) vibration frequency, it concerns the symmetric stretching in the *ab* plane of the Ge-O1 bonds and the twisting motion of O2-K-O2 bridges, Figure 4. Both K and Sb atoms are fixed.

The O1-Ge-O1 wagging of the Ge_3O_3 central cycle along the *c* axis and the O2-K-O2 wagging of the KO_6 octahedra occur in the A''_2(TO) band at 812 cm^{-1} which is only IR active, Table 5 and Figure 4.

For this mode, the dominant motions are due to both the Ge atoms forming the Ge_3O_3 rings and the O2 atoms. The displacement of the Sb atoms is small while that of K is null.

The 848 cm^{-1} E'(TO) theoretical vibration, Table 5, is due to intra-cycle symmetric stretching motions of the O1 atoms concomitant to the shear in the *ab* plane of the ring Ge_3O_3 and the O2-K-O2 twisting, Figure 4. The Sb and K atoms do not move.

The 937 cm^{-1} calculated frequency which is both IR and Raman active (E'(TO), Table 5) is attributed to the Ge-O1 symmetric stretching in the Ge_3O_3 ring and the vibration associated with the rotation of whole KO_6 octahedra (libration mode), Figure 4. The Sb and K atoms do not move.

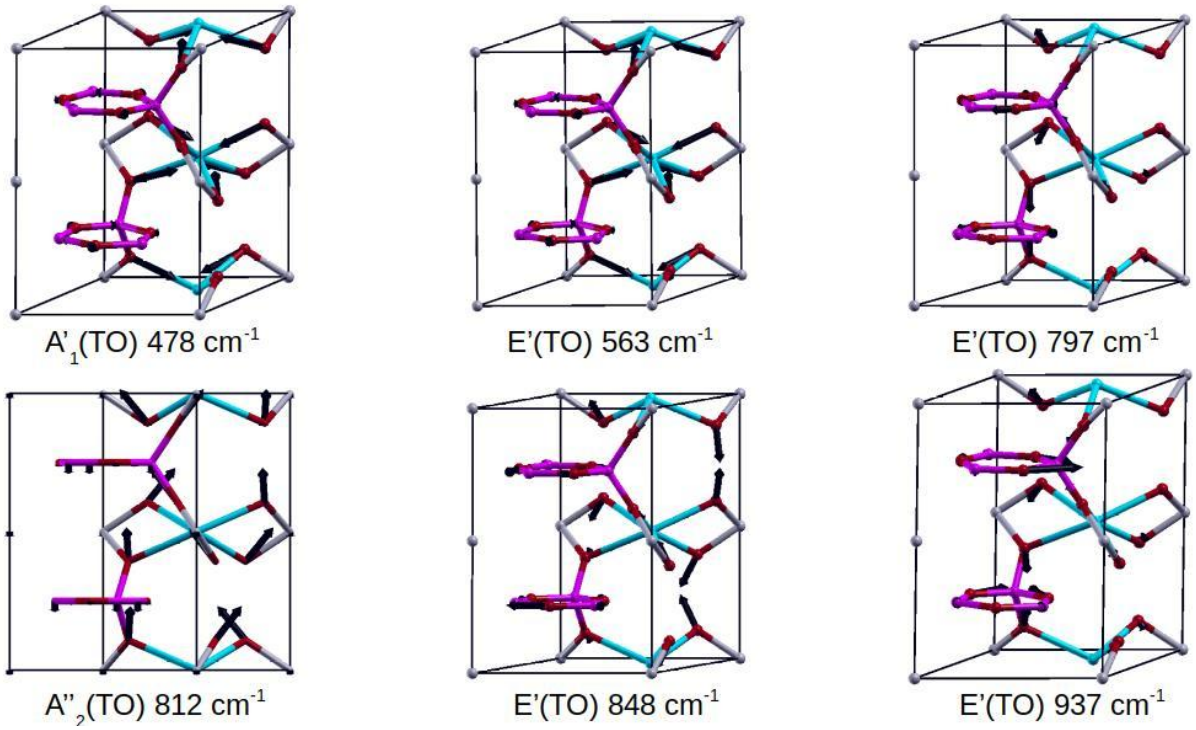

Figure 4. Atomic motions of some vibrations in the non-centrosymmetric $KSbGe_3O_9$ compound

4. CONCLUSION

The structural and vibrational properties of the hexagonal $KSbGe_3O_9$ crystal have been studied for the first time by using experimental data combined with first-principles based calculations. The main conclusions are the following:

(1) This non-centrosymmetric phase ($P\bar{6}c2$) is visually colorless and transparent, and it is structurally stable from room-temperature up to, at least, 1200°C.

(2) The unit cell parameters refined from X-ray single-crystal data are different from those given in JCPDS card number 00-038-1334.

(3) $KSbGe_3O_9$, with planar Ge_3O_3 rings, belongs to the benitoite-type structure.

(4) The observed IR and Raman band positions are in good agreement with the calculated ones.

(5) The structural origin of the most intense vibrations is mainly due to the oxygen motions.

(6) Two E'(TO) vibrations (IR and Raman active) characterize the planarity of the Ge_3O_3 ring in the *ab* plane.

This anisotropic oxide with stoichiometric chemical composition and large thermal structure stability may have potential piezo-electrical and non-linear optical properties exploitable in a range of very high temperatures up to, at least, 1200°C. Lead-free materials that can operate under extreme stress without degradation are sought for industrial needs. Furthermore, this germanate with its open-framework structure and well-defined channels may be suitable for ion-exchange and gas adsorption applications.

Acknowledgments

The EDX experiments were conducted at the Plateau Technique Microscopie à Balayage at the IEM Institute in Montpellier, France. IR, Raman and single-crystal X-ray diffraction experiments were done at the Platform of Analysis and Characterization of the Pôle Chimie Balard in Montpellier, France.

Funding information

Funding for this research was provided by the Ministry of Higher Education, Scientific Research and Innovation in France, and the French National Center of Scientific Research (CNRS).

REFERENCES

[1] Czochralski growth, defect analysis and refractive index of $Ba_2TiGe_2O_8$ crystal with excellent optical nonlinearities
Liu, XF; Huo, LN ; Liao, BY; Wei, QK; Hu, XL; Zhuang, NF; Chen, JZ; Huang, LX; Zhang, G
Opt. Mater. 42 (2015) 361-365.

[2] $Cs_2Bi_2O(Ge_2O_7)$ (CBGO): A Larger SHG Effect Induced by Synergistic Polarizations of BiO_5 Polyhedra and GeO_4 Tetrahedra
Tang, RL; Hu, CL ; Wu, BL; Fang, Z ; Chen, Y ; Mao, JG
Angew. Chem. Int. Ed. 58 No.43 (2019) 15358-15361
DOI: 10.1002/anie.201909735

[3] Optical properties of the germanate melilites $Sr_2MgGe_2O_7$, $Sr_2ZnGe_2O_7$ and $Ba_2ZnGe_2O_7$
Becker, P.; Held, P.; Liebertz, J.; et al.
Cryst. Res. Technol. 44 No. 6 (2009) 603-612.

[4] Piezoelectric and Nonlinear Optical Properties of $PbGe_4O_9$ Crystals
A. A. Bush, S. Yu. Stefanovich
Inorg. Mater. 38 No.2 (2002) 168-171. Translated from Neorganicheskie Materialy, 38(2) (2002) 221-225.

[5] Electromechanical Properties of $Pb_3Ga_2Ge_4O_{14}$ Piezoelectric Crystals Grown from Solution in a Melt
B. P. Sorokin, D. A. Glushkov, L. N. Bezmaternykh, V. L. Temerov, I. A. Gudim, and K. S. Aleksandrov

Phys. Solid State 46(3) (2004) 458–461. Translated from Fizika Tverdogo Tela 46No. 3 (2004) 446–448.

[6] High temperature piezoelectric properties of flux-grown α-GeO_2 single crystal
P. Papet, M. Bath, A. Haidoux, B. Ruffle, B. Menaert, A. Peña, J. Debray, P. Armand
J. Appl. Phys. 126 (2019) 144102.

[7] Density Functional Theory Predictions of the Nonlinear Optical Properties in α-Quartz-type Germanium Oxide
P. Hermet, G. Fraysse, A. Lignie, P. Armand and Ph. Papet
J. Phys. Chem. C 116 (2012) 8692-8698.

[8] Oxides with a tunnel structure characterized by a mixed framework of octahedra and tetrahedra
B. Raveau
Proc. Indian Acad. Sci. (Chem. Sci.) 96 (1986) 419-448.

[9] Space formations and nonlinear properties of noncentrosymmetric germanates
Anton Sergeevich Korotkov
J. Solid State Che. 218 (2014) 141-145.

[10] The Crystal Structure of Benitoite, $BaTiSi_3O_9$
W. H. Zachariasen
Z. Kristallogr. Cryst. Mater 74 (1930) 139–146.

[11] Sur de nouveaux germanates et silicates de type Bénitoïte
J. Choisnet, A. Deschanvres, B. Raveau
J. Solid State Chem. 4 (1972) 209-2018.

[12] Synthèse et évolution structurale de nouveaux silicogermanates $BaGe(Ge_{3-x}Six)O_9$ de type benitoïte et de structure apparentée
M. Goreaud, J. Choisnet, A. Deschanvres, B. Raveau
Mat. Res. Bull. 8 (1973) 1205-1214.

[13] A potential red-emitting Phosphor $BaZrGe_3O_9$:Eu3+ for WLED and FED applications: Synthesis, structure and luminescence properties
Q. Zhang, X. Wang, X. Ding, Y. Wang
Inorg. Chem. 56 (2017) 6990-6998.

[14] Raman spectroscopic study of benitoite-type compounds
Y. Takahashi, K. Iwasaki, H. Masai, T. Fujiwara
J. Ceram. Soc. Jpn. 116 (2008) 1139-1142.

[15] The Compound $BaTiGe_3O_9$
R. Robbins
J. Am. Ceram. Soc. 43(11) (1960) 610-610.

[16] New strategy for designing promising mid-infrared nonlinear optical materials: narrowing the band gap for large nonlinear optical efficiencies and reducing the thermal effect for a high laser-induced damage threshold‡
Shu-Fang Li, Xiao-Ming Jiang, Yu-Hang Fan, Bin-Wen Liu, Hui-Yi Zeng, Guo-Cong Guo
Chem. Sci. 9(26) (2018) 5700–5708.

[17] Single-crystal growth, structure, and optical properties of a new non-centrosymmetric germanate, $RbSbGe_3O_9$
P. Armand, M. Tillard, A. Haidoux, L. Daenens.
J. Solid State Chem. 286 (2020) 121290
DOI : 10.1016/j.jssc.2020.121290

[18] ABINIT: First-principles approach to material and nanosystem properties
X. Gonze, B. Amadon, P.M. Anglade, et al.,
Comput. Phys. Comm. 180 (2009) 2582-2615.
DOI :10.1016/j.cpc.2009.07.007
[19] Accurate and simple analytic representation of the electron-gas correlation energy
J.P. Perdew, Y. Wang,
Phys. Rev. B. 45 (1992) 13244–13249.

DOI:10.1103/physrevb.45.13244

[20] Special points for Brillouin-zone integrations
H.J. Monkhorst, J.D. Pack
Phys. Rev. B 13 (1976) 5188−5192.
https://doi.org/10.1103/PhysRevB.13.5188

[21] Nonlinear optical susceptibilities, Raman efficiencies, and electro-optic tensors from first-principles density functional perturbation theory
M. Veithen, X. Gonze, P. Ghosez
Phys. Rev. B 71 (2005) 125107.
https://doi.org/10.1103/PhysRevB.71.125107

[22] The joint Committee on Powder Diffraction Standards Card N° 00-038-1334.

[23] *Crystal structure refinement with SHELXL*
G. M. Sheldrick
Acta Cryst. C71 (2015) 3-8
https://doi.org/10.1107/S2053229614024218

[24] SHELXT - Integrated space-group and crystal-structure determination
G. M. Sheldrick
Acta Cryst. A71 (2015) 3-8
https://doi.org/10.1107/S2053273314026370

[25] http://www.ccdc.cam.ac.uk/conts/retrieving.html (or from the CCDC, 12 Union Road, Cambridge CB2 1EZ, UK; Fax: +44 1223 336033; E-mail: deposit@ccdc.cam.ac.uk).

[26] Diamond - Crystal and Molecular Structure Visualization
Crystal Impact - Dr. H. Putz & Dr. K. Brandenburg GbR, Kreuzherrenstr. 102, 53227 Bonn, Germany
http://www.crystalimpact.com/diamond

[27] Spectres vibrationnels des silicates et germanates renfermant des anneaux, M_3O_9 (M=Si, Ge)-I. Attribution des fréquences caractéristiques de l'anneau M_3O_9 dans les composés de type bénitoïte, wadéite et tétragermanate.
J. Choisnet, A. Deschanvres, P. Tarte
Spectrochim. Acta A 31 (1975) 1023-1034.

[28] Crystal structure and optical properties of germanates $Ln_2Ca(GeO_3)_4$ (Ln= Gd, Ho, Er, Yb, Y)
V.G. Zubkov, I.I. Leonidov, A.P. Tyutyunnik, N.V. Tarakina, I.V. Baklanova, L.A. Perelyaeva, L.L. Surat
Physics of the solid state 50 (2008) 1699-1706.

[29] FT-IR studies of cyclogermanates
M. Sitarz, M. Handke, H.H. Otto
Vibrationnal Spectroscopy 29 (2002) 45-51.